Introducing new lightning schemes into the CHASER (MIROC) chemistry climate model

Yanfeng He[1], Hossain Mohammed Syedul Hoque[1], Kengo Sudo[1,2]
[1] Graduate School of Environment Studies, Nagoya University, Nagoya, 464-8601, Japan
5 [2] Japan Agency for Marine–Earth Science and Technology (JAMSTEC), 237-0061, Yokohama, Japan

Correspondence to: Yanfeng He (hyf412694462@gmail.com)

Abstract. The formation of nitrogen oxides (NO_x) associated with lightning activities (hereinafter designated as LNO_x) is a major source of NO_x. In fact, it is regarded as the most dominant NO_x source in the upper troposphere. Therefore, improve the prediction accuracy of lightning and LNO_x in chemical climate models is crucially important. This study implemented two

10   new lightning schemes with the CHASER (MIROC) global chemical transport/climate model. The first lightning scheme is based on upward cloud ice flux (ICEFLUX scheme), whereas the second, also adopted in the European Centre for Medium-Range Weather Forecasts (ECMWF) forecasting system (original ECMWF scheme). In the case of the original ECMWF scheme, by tuning the equations and adjustment factors for land and ocean, a modified ECMWF scheme was also tested in CHASER. In the original version of CHASER (MIROC), lightning is initially parameterized with the widely used cloud top

15   height scheme (CTH scheme). Model evaluations with lightning observations conducted using an optical transient detector (OTD) indicate that both the ICEFLUX and ECMWF schemes simulate the spatial distribution of lightning more accurately on a global scale than the CTH scheme does. The modified ECMWF scheme showed the highest prediction accuracy for the global distribution of lightning. Validation by atmospheric tomography (ATom) aircraft observations and tropospheric monitoring instrument (TROPOMI) satellite observations shows that the ICEFLUX scheme reduced the model biases to a

20   greater extent than the ECMWF schemes when compared using the CTH scheme. The effects of the newly introduced lightning schemes on the tropospheric chemical fields were evaluated by comparison with the CTH scheme. Although the newly implemented lightning schemes have a minor effect on the tropospheric mean oxidation capacity compared to the CTH scheme, they led to marked change of oxidation capacity in different regions of the troposphere. Long-term trend analyses of flash and surface temperatures predicted using CHASER (2001–2020) show that lightning schemes predicted an increasing trend of

25   lightning, except for the ICEFLUX scheme, which predicted a decreasing trend of lightning. The global lightning rates of increase during 2001–2020 predicted by the CTH scheme were 17.86%/°C and 2.60%/°C, respectively, with and without nudging, which are slightly beyond the range of an earlier study (5%/°C–16%/°C). Furthermore, the ECMWF schemes predicted a larger increasing trend of lightning flash rates under global warming by a factor of 3 (modified ECMWF scheme) and 5 (original ECMWF scheme) compared to the CTH scheme without nudging. In conclusion, the two new lightning schemes

30   improved global lightning prediction in the CHASER model. However, further research is needed to assess the reproductivity of long-term trends of lightning.

Keywords

lightning, lightning scheme, lightning NO_x, chemistry-climate model, lightning under climate change

1 Introduction

35   Reactive nitric oxide (NO) can be formed during lightning activities. Also, NO can be oxidized quickly to nitrogen dioxide (NO_2). An equilibrium between NO and NO_2 can be reached during daytime. Those gases are known collectively as NO_x (Finney, 2014). Actually, LNO_x is estimated as contributing approximately 10% of the global NO_x source. Regarded as the most dominant NO_x source in the upper troposphere (Schumann and Huntrieser, 2007; Finney et al., 2016a), NO_x is associated with many chemical reactions in the atmosphere. Most importantly, NO reacts with peroxy radical to reproduce

40 OH radical. Photochemical dissociation of NO_2 engenders the production of ozone (Isaksen and Hov, 1987; Grewe, 2007). The primary oxidants in the atmosphere, which are OH radical and ozone, control the oxidation capacity of the atmosphere. Results of several studies have indicated that global-scale LNO_x emissions are an important contributor to ozone and other trace gases, especially in the upper troposphere (Labrador et al., 2005; Wild, 2007; Liaskos et al., 2015). Consequently, LNO_x influences atmospheric chemistry and global climate to a considerable degree (Schumann and Huntrieser, 2007;

45 Murray, 2016; Finney et al., 2016b; Tost, 2017). However, large uncertainties remain in predicting lightning and LNO_x in chemical climate models (Tost et al., 2007). Therefore, improving lightning prediction accuracy and quantifying LNO_x in chemical climate models is crucially important for future atmospheric research.

Chemical climate models such as CHASER (MIROC) (Sudo et al., 2002; Sudo and Akimoto, 2007; Watanabe et al., 2011)
50 most often use the convective cloud-top height to parameterize the lightning flash rate (Price and Rind, 1992; Lamarque et al., 2013). However, some new lightning schemes have been devised to simulate better the spatial and temporal correlation and root mean square error (RMSE) compared to the spaceborne Lightning Imaging Sensor (LIS) and Optical Transient Detector (OTD) lightning observation data (Finney et al.,2014; Lopez 2016). A lightning scheme proposed by Finney (2014), which is based on upward cloud ice flux, has shown better spatial and temporal correlation coefficients and RMSEs

55 than the cloud top height scheme compared against the LIS/OTD lightning observations. Another lightning scheme also showed more accurate lightning prediction than the cloud top height scheme, which is also adopted in the ECMWF forecasting system (Lopez, 2016). The two new lightning schemes described above have only been validated in a few chemical transport and climate models. The new lightning schemes must be validated and compared in more chemical transport and climate models, such as CHASER. To achieve better prediction accuracy for lightning and better quantification

60 of LNO_x in chemical climate models, comparing and optimizing the existing lightning schemes and validating them with various observation data are also important.

Lightning simulations are also fundamentally important in chemical climate model studies for predictions of atmospheric chemical fields and climate. Nevertheless, different lightning schemes respond very differently on decadal to multi-decadal
65 time scales under global warming. Some lightning schemes such as those using cloud top height or convective available potential energy (CPAE) × precipitation as a proxy for calculating lightning indicate that lightning increases concomitantly with increasing global average temperature. By contrast, other lightning schemes, such as those using convective mass flux or upward cloud ice flux as a proxy of lightning, indicate that lightning will decrease as the global average temperature increases (Clark et al., 2017; Finney et al., 2018). Several studies (Price and Rind 1994; Zeng et al., 2008; Jiang and Liao

70 2013; Banerjee et al., 2014; Krause et al., 2014; Clark et al., 2017) have found 5–16% increases in lightning flashes per degree of increase in global mean surface temperatures with the lightning scheme based on cloud top height. Over the continental United States (CONUS), the CAPE × precipitation proxy predicted a 12 ± 5% increase in the CONUS lightning flash rate per degree of global mean temperature increase (Romps et al., 2014). By contrast, Finney et al. (2018) found a 15% global mean lightning flash rate decrease with the lightning scheme based on upward cloud ice flux in 2100 under a

75 strong global warming scenario. Furthermore, a 2.0% decrease in global mean lightning flashes per degree of increase in the global mean surface temperature with the lightning scheme based on convective mass flux has been reported by Clark et al. (2017). Although it remains unclear which lightning scheme is best suited to predicting future lightning (Romps, 2019), comparing different lightning schemes in different chemical climate models is valuable for consideration of the sensitivity of lightning to global warming.

80

This study introduced two new lightning schemes into CHASER (MIROC). The first lightning scheme (Finney et al., 2014) is based on upward cloud ice flux. The second one (Lopez, 2016), also adopted in the ECMWF forecasting system,

calculates lightning flash rates as a function of the frozen precipitation convective flux, CAPE, and convective cloud-base
height. In the case of the second lightning scheme, by tuning the equations and adjustment factors based on a study reported
85 by McCaul et al. (2009), a new modified version of the second lightning scheme was also tested for CHASER (MIROC).
This study conducted detailed validation of lightning and LNO_x by LIS/OTD lightning observations, NASA/ATom aircraft
observations, and TROPOMI satellite observations. The effects of different lightning schemes on the atmospheric chemical
fields were evaluated. Also, 20-year (2001–2020) long-term trend analyses of lightning densities and LNO_x emissions
simulated by different lightning schemes were conducted. Based on the results, the effects of LNO_x emissions during 2001–
90 2020 on tropospheric NO_x and O_3 column trends were estimated and discussed.

Research methods, including the model description and experiment setup, are described in section 2. In section 3.1,
validation of lightning schemes using LIS/OTD lightning observations is explained. In section 3.2, LNO_x emission
simulation by different lightning schemes is verified with aircraft and satellite measurements. Section 3.3 presents discussion
95 of the effects of different lightning schemes on the atmospheric chemical fields. Long-term trends of lightning simulated by
different lightning schemes are analyzed and discussed in section 3.4. Section 3.5 discussed how LNO_x emissions (2001–
2020) trends influence the tropospheric NO_x and O_3 column trends. Section 4 presents the conclusions obtained from this
study.

2 Method

2.1 Chemistry-climate model

The model used for this study is the CHASER (MIROC) global chemical transport and climate model (Sudo et al., 2002;
Sudo and Akimoto, 2007; Watanabe et al. 2011; Ha et al., 2021), which incorporates consideration of detailed chemical and
transport processes in the troposphere and stratosphere. CHASER calculates the distributions of 94 chemical species and
reflects the effects of 269 chemical reactions (58 photolytic, 190 kinetic, 21 heterogeneous). Its tropospheric chemistry
105 incorporates consideration of Non-Methane Hydrocarbons (NMHC) oxidation and the fundamental chemical cycle of O_x–
NO_x–HO_x–CH_4–CO. Its stratospheric chemistry simulates chlorine-containing and bromine-containing compounds,
chlorofluorocarbons (CFCs), hydrofluorocarbons (HFCs), carbonyl sulfide (OCS), and N_2O. Furthermore, it simulates the
formation of polar stratospheric clouds (PSCs) and heterogeneous reactions on their surfaces. CHASER is coupled to the
MIROC AGCM ver. 5.0 (Watanabe et al., 2011). Grid-scale large-scale condensation and cumulus convection (Arakawa–
110 Schubert scheme) are used to simulate cloud/precipitation processes. Aerosol chemistry is coupled with the SPRINTARS
aerosol model (Takemura et al., 2009), which is also based on MIROC.

For this study, horizontal resolution used is T42 (2.8° × 2.8°), with vertical resolution of 36 σ-p hybrid levels from the
surface to approximately 50 km. The AGCM meteorological fields (u, v, T) simulated by MIROC were nudged towards the
115 six-hourly NCEP FNL data (https://rda.ucar.edu/datasets/ds083.2/, last access: 6 December 2021). Anthropogenic precursor
emissions such as NO_x, CO, O_3, SO_2, and VOCs were obtained from the HTAP-II inventory for 2008
(https://edgar.jrc.ec.europa.eu/dataset_htap_v2, last access: 6 December 2021), with biomass burning emissions from
MACC-GFAS (Inness et al., 2013).

2.2 Lightning NOx emission scheme

120 The lightning flash rate in CHASER is originally parameterized by cloud-top height (Price and Rind, 1992, 1993), with a "C-
shaped" NO_x vertical profile adopted (Pickering et al., 1998). The equations used to calculate the lightning flash rate by
cloud-top height are

$$F_l = 3.44 \times 10^{-5} H^{4.9} \tag{1}$$
$$F_o = 6.2 \times 10^{-4} H^{1.73} \tag{2}$$

125 where F represents the total flash frequency (fl. min⁻¹), H stands for the cloud-top height (km), and subscripts l and o respectively denote the land and ocean (Price and Rind, 1992).

For this study, two new lightning schemes are implemented into CHASER (MIROC). One is based on upward cloud ice flux. It calculates the lightning flash rate by the following equations, as described by Finney et al. (2014).

130 $$f_l = 6.58 \times 10^{-7} \phi_{ice} \tag{3}$$
$$f_o = 9.08 \times 10^{-8} \phi_{ice} \tag{4}$$

Therein, f_l and f_o respectively represent the flash density (fl. m⁻² s⁻¹) of land and ocean. Also, ϕ_{ice} is the upward cloud ice flux at 440 hPa (kg$_{ice}$ m$_{cloud}^{-2}$ s⁻²) as calculated using

$$\phi_{ice} = \frac{q \times \Phi_{mass}}{c}, \tag{5}$$

135 where q denotes the specific cloud ice water content at 440 hPa (kg$_{ice}$ kg$_{air}^{-1}$), Φ_{mass} stands for the updraught mass flux at 440 hPa (kg$_{air}$ m$_{cell}^{-2}$ s⁻¹), and c represents the fractional cloud cover at 440 hPa (m$_{cloud}^2$ m$_{cell}^{-2}$).

Another new lightning scheme, also adopted in the ECMWF forecasting system, calculates lightning flash rates as a function of the frozen precipitation convective flux, CAPE, and convective cloud-base height (Lopez, 2016) as

140 $$f_T = \alpha Q_R \sqrt{CAPE} \min(z_{base}, 1.8)^2, \tag{6}$$

where f_T is the total lightning flash density (fl. km⁻² day⁻¹), z_{base} is the convective cloud-base height in km, α is a constant obtained after calibration against the OTD climatology, which is set to 95.58 in this study. $CAPE$ is diagnosed from the following equation.

$$CAPE = \int_{z_{LFC}}^{z_{w=0}} \max(g \frac{T_v^u - \overline{T_v}}{\overline{T_v}}, 0) dz \tag{7}$$

145 In that equation, g is the constant of gravity. Also, T_v^u and $\overline{T_v}$ respectively denote the virtual temperatures in the updraft and the environment. The integral in equation (7) starts at the level of free convection z_{LFC} and stops at the level at which negative buoyancy is found ($w = 0$). Quantity Q_R is intended to represent the charging rate of collisions between graupel and other types of hydrometeors inside the charge separation region. It is empirically calculated as

$$Q_R = \int_{z_0}^{z_{-25}} q_{graup}(q_{cond} + q_{snow})\bar{\rho} dz, \tag{8}$$

150 where z_0 and z_{-25} signify the heights of the 0° and -25°C isotherms, and q_{cond} denotes the mass mixing ratio of cumulus cloud liquid water (kg kg⁻¹). The respective amounts of graupel (q_{graup}; kg kg⁻¹) and snow (q_{snow}; kg kg⁻¹) are computed from the following equations for each vertical level of the model.

$$q_{graup} = \beta \frac{P_f}{\bar{\rho} V_{graup}} \tag{9}$$
$$q_{snow} = (1 - \beta) \frac{P_f}{\bar{\rho} V_{snow}} \tag{10}$$

155 In those equations, P_f denotes the vertical profile of the frozen precipitation convective flux (kg m⁻² s⁻¹), $\bar{\rho}$ stands for the environmental air density (kg m⁻³), and V_{graup} and V_{snow} respectively express the typical fall speeds for graupel and snow set to 3.0 and 0.5 m s⁻¹. The dimensionless coefficient β is set as 0.7 for land and 0.45 for ocean to account for the observed lower graupel contents over oceans.

160 For the original ECMWF scheme, by tuning the convective cloud-base height, the calculation equations, and the adjustment factors for land and ocean, the lightning prediction accuracy is improved further, as explained in Section 3.1. The modified ECMWF scheme simulates the lightning flash rate by the following equations.

$$f_l = \alpha_l Q_{Ra} CAPE^{1.3} \tag{11}$$

$$f_o = \alpha_o Q_{Ra} CAPE^{1.3} \tag{12}$$

165 Therein, f_l and f_o respectively denote the total flash density of land and ocean. Also, α_l and α_o are constants obtained after calibration against LIS/OTD climatology, respectively, for land and ocean. For this study, α_l and α_o are set respectively to 2.36×10^{-5} and 1.45×10^{-6}. Then $CAPE$ is computed in the same way as the original ECMWF scheme. In addition, Q_{Ra} is a proxy for the charging rate resulting from the collisions between graupel and hydrometeors of other types inside the charge separation region (from 0° to -25°C isotherm), as reported by McCaul et al. (2009). Also, Q_{Ra}

170 represents the total volumetric amount of precipitating ice in the charge separation region, calculated as

$$Q_{Ra} = \int_{z_0}^{z_{-25}} (q_{graup} + q_{snow} + q_{ice}) \bar{\rho} dz, \tag{13}$$

where z_0 and z_{-25} respectively stand for the heights of the 0° and -25°C isotherms, and q_{graup}, q_{snow}, and q_{ice} respectively represent the mass mixing ratios of graupel, snow, and cloud ice. In this study, q_{graup} and q_{snow} were computed respectively by equations (9) and (10). For the modified ECMWF scheme, V_{graup} and V_{snow} are set respectively

175 to 3.1 and 0.5 m s^{-1}. Then q_{ice} was diagnosed using Arakawa–Schubert cumulus parameterization.

Table 1: Basic information of all lightning schemes assessed for this study

Abbreviation	Parameter	Remark
CTH (Price, C., & Rind, D., 1994)	Cloud top height	Originally used in CHASER (MIROC)
ICEFLUX (Finney et al., 2014)	Upward cloud ice flux at 440 hPa	The 440 hPa level is used as a pressure level representative of fluxes in deep convective clouds
ECMWF-original (Lopez, 2016)	• CAPE • Convective cloud-base height • Frozen precipitation convective flux • Mixing ratio of cumulus cloud liquid water	Also adopted in the ECMWF forecasting system
ECMWF-mod	• CAPE • Frozen precipitation convective flux • Mixing ratio of cumulus cloud ice	Equations and adjustment factors are modified from the original ECMWF scheme. Equations are modified based on findings reported by McCaul (McCaul Jr, E. W. et al., 2009)

Table 1 presents all the lightning schemes examined for this study. As described in this paper, the original ECMWF scheme and the modified ECMWF scheme are designated collectively as ECMWF schemes. The NO emission per flash used in

180 CHASER for all the introduced lightning schemes was set to 111 moles NO per intra-cloud (IC) lightning flash and 1113 moles NO per cloud-to-ground (CG) lightning flash as parameters, as explained by Price et al. (1997). A fourth-order polynomial is used to calculate the proportion of total flashes that are cloud-to-ground (p) based on the cold depth, as described in an earlier report (Price and Rind, 1993).

$$p = \frac{1}{64.09 - 36.54D + 7.493D^2 - 0.648D^3 + 0.021D^4}. \tag{14}$$

185 In that equation, D represents the cloud depth above 0°C in kilometres.

A "C-shaped" vertical profile for LNO$_x$ emission is used initially in CHASER (MIROC). However, a recent report of work by Ott et al. (2010) indicated that a "C-shaped" vertical profile of LNO$_x$ might place too much mass near the surface and too little in the middle troposphere. A new LNO$_x$ vertical profile named the "backward C-shaped" profile was subsequently

190 proposed by Ott et al. (2010). It was tested in this study using CHASER (MIROC).

2.3 Observation data for model evaluation

2.3.1 Lightning observations

The LIS/OTD gridded climatology datasets are used for this study, consisting of climatologies of total lightning flash rates observed using the Lightning Imaging Sensor (LIS) and spaceborne Optical Transient Detector (OTD): OTD aboard the

195 MicroLab-1 satellite and LIS aboard the Tropical Rainfall Measuring Mission (TRMM) satellite (Cecil et al., 2014). Both sensors detect lightning by monitoring pulses of illumination produced by lightning in the 777.4 nm atomic oxygen multiplet above background levels. Both sensors, in low earth orbit, view an earth location for about 3 min as OTD passes overhead or for 1.5 min as LIS passes overhead. Actually, OTD and LIS circle the globe 14 times a day and 16 times a day, respectively.

OTD collected data between +75 and -75° latitude from May 1995 through March 2000, whereas LIS observed between +38

200   and -38° latitude from January 1998 through April 2015.

The product used throughout this paper is the LIS/OTD 2.5 Degree Low Resolution Time Series (LRTS). The LRTS
includes the daily lightning flash rate on a 2.5° regular latitude–longitude grid from May 1995 through April 2015.
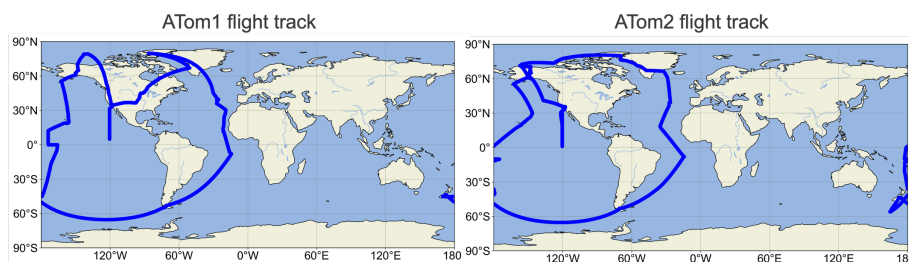
Figure 1: ATom1 and ATom2 flight tracks.

205

2.3.2 Atmospheric tomography (ATom) aircraft observations

To validate the LNO_x emissions calculated by different lightning schemes, we used NO observation by the atmospheric
tomography (ATom) aircraft missions (Wofsy et al., 2018). By deploying an extensive gas and aerosol payload on the
NASA DC-8 aircraft, ATom is designed to sample the atmosphere systematically on a global scale, performing continuous

210   profiling from 0.2 to 12 km altitude. Flights took place in each of the four seasons of 2016 through 2018. To validate the
LNO_x emissions in different seasons, ATom1 (July–August 2016) and ATom2 (January–February 2017) were used for
validation. Both ATom1 and ATom2 originate from the Armstrong Flight Research Center in Palmdale, California, USA, fly
north to the western Arctic, south to the South Pacific, east to the Atlantic, north to Greenland, and return to California
across central North America. Figure 1 exhibits the respective flight tracks of ATom1 and ATom2.

215   ### 2.3.3 TROPOMI satellite observations

Tropospheric Monitoring Instrument (TROPOMI) is the payload on-board the Sentinel-5 Precursor (S5P) satellite of the
European Space Agency (ESA), which was launched in October 2017. TROPOMI has been providing observations of
important atmospheric pollutants (NO_2, O_3, CO, CH_4, SO_2, CH_2O) with an unprecedented horizontal resolution of approx. 7
$\times$ 3.5 km^2 since August 2017 (changed to 5.5 $\times$ 3.5 km^2 after August 2019). For this study, the TROPOMI observations in

220   2019 for the NO_2 tropospheric column were used to validate the LNO_x emissions simulated by different lightning schemes.

2.4 Experiment setup

For this study, all the introduced lightning schemes were implemented into CHASER (MIROC). Six sets of experiments
were conducted for this study, as presented in Table 2. For each set of experiments, the same initial conditions and chemical
emissions were used except for LNO_x emissions. The set of experiments that applied meteorological nudging also has the

225   same meteorological conditions. The first set of experiments was conducted for the years of 2001–2020. It was used to
validate the distribution of the lightning flash rate against LIS/OTD lightning observations and to derive the long-term
lightning trend. The second set of experiments is the same as the first set of experiments, but using daily mean LNO_x
emission rates of 2001 calculated using lightning schemes for each year. This set of experiments is used to produce results
for comparison with those of the first set of experiments to estimate the effects of LNO_x emission trends on tropospheric

230   NO_x and O_3 column trends. The third set of experiments gives results for 2011–2020. These experiments are used to estimate
the effects of different lightning schemes on atmospheric chemical fields. To normalize the different annual LNO_x emission
amounts by different lightning schemes, the mean LNO_x production (2011–2020) of all lightning schemes was adjusted to

5.0 TgN yr^{-1} using different adjustment factors. The fourth set of experiments is for 2016, with the fifth set is for 2017. These two sets of experiments were conducted to compare model results with ATom1 and ATom2 aircraft observations. The sixth

235   set of experiments is for 2019. It is conducted to validate model results using TROPOMI satellite observations.

Table 2: All experiments in this study

Number	Period	Nudging	LNO$_x$ emissions	Adjusted to 5.0 TgN yr^{-1}
1st	2001–2020	On	Interactively calculated	No
	2001–2020	Off	Interactively calculated	No
2nd	2001–2020	On	Fixed to 2001	No
	2001–2020	Off	Fixed to 2001	No
3rd	2011–2020	On	Interactively calculated	Yes
4th	2016	On	Interactively calculated	Yes
5th	2017	On	Interactively calculated	Yes
6th	2019	On	Interactively calculated	Yes

All experiments used the "backward C-shaped" LNO$_x$ vertical profile. The NO emissions per flash were set to 111 moles NO per IC (intro-cloud lightning flash) and 1113 moles NO per CG (cloud-to-ground lightning flash) as parameters drawn from

240   work reported by Price et al. (1997).

3 Results and Discussion

3.1 Validation of the lightning schemes

To validate model results with lightning observation data in a broader range (between +75° and -75° latitude), lightning prediction accuracy for all introduced lightning schemes was compared with the climatological lightning distributions of

245   OTD (1996–2000). Figure 2 presents a global map of the OTD annual mean lightning density spanning 1996–2000 and mean lightning density during 2007–2011, as simulated using different lightning schemes. Figure 3 displays a Taylor diagram, which presents the prediction accuracy of various lightning schemes in 2007–2011 simulations compared to the OTD 1996–2000 lightning climatology. Figure 2 shows that lightning over the ocean is not well reproduced by the original CTH scheme. Actually, it is improved considerably by the new lightning schemes. Compared with the CTH scheme, the

250   original ECMWF scheme better represents the lightning distribution in South Asia including the Indian region. The ECMWF schemes and the ICEFLUX scheme reduced negative biases in North America compared to the CTH scheme. In Australia, the ECMWF schemes better simulate the horizontal distribution of lightning. All lightning schemes failed to capture the worldwide maximum value found over the Congo Basin, although all lightning schemes captured the active region in central Africa.
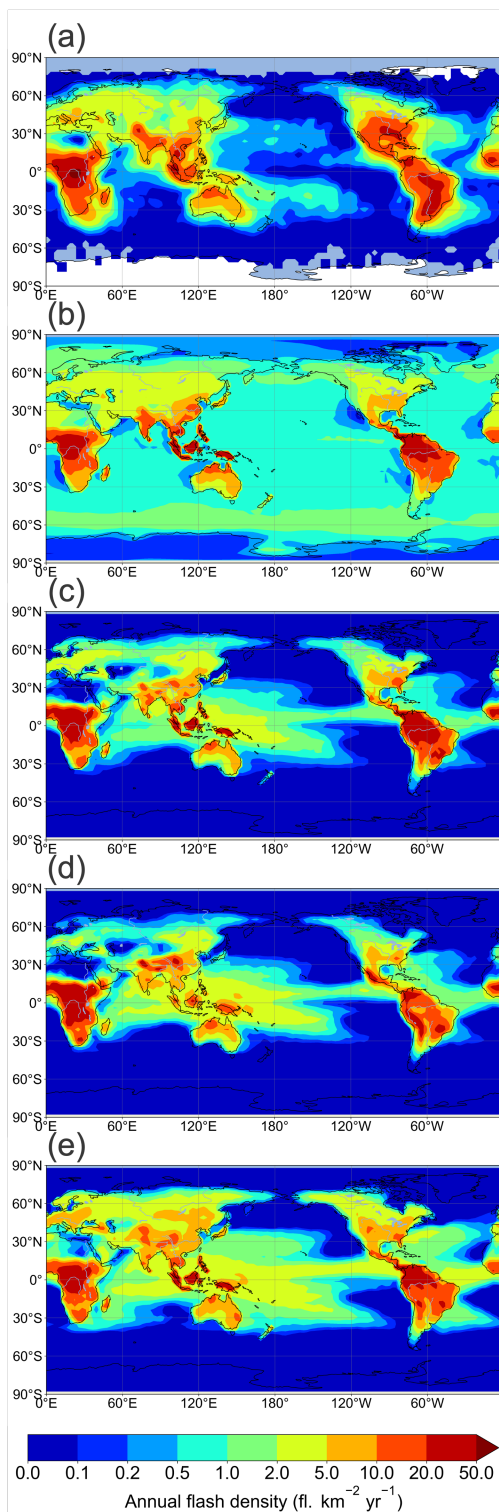
255

Figure 2: Annual mean lightning flash densities from (a) OTD satellite observations spanning 1996–2000, (b) the CTH scheme in 2007–2011, (c) the modified ECMWF scheme in 2007–2011, (d) the original ECMWF scheme in 2007–2011, and (e) the ICEFLUX scheme in 2007–2011.
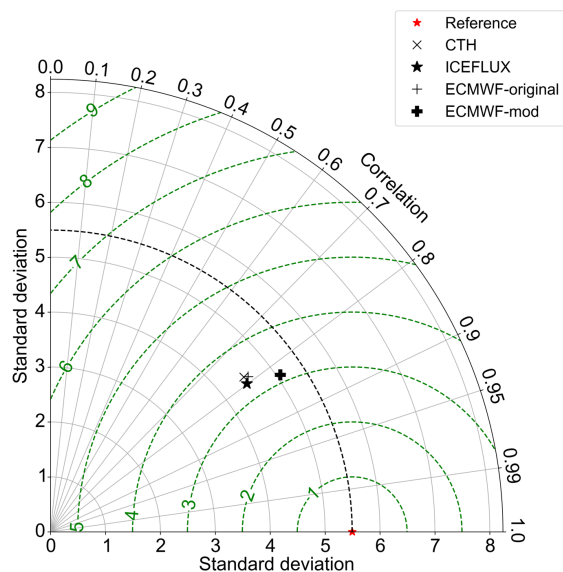
Figure 3: Taylor diagram showing the prediction accuracy of various lightning schemes in 2007–2011 simulations compared to the OTD 1996–2000 lightning climatology.

In Fig. 3, comparison of the annual mean lightning flash rate of OTD 1996–2000 and the CHASER calculation for 2007–2011 yields spatial correlation coefficients of 0.80 and 0.79 for the ICEFLUX and original ECMWF schemes, respectively, which are slightly higher than that found for the CTH scheme (0.78). The RMSE of the ICEFLUX scheme is 3.31 fl. km^{-2} yr^{-1}, which is slightly less than that of the CTH scheme of 3.44 fl. km^{-2} yr^{-1}. Among all lightning schemes, the modified ECMWF scheme exhibits the highest spatial correlation coefficient (0.83) and the lowest RMSE (3.20 fl. km^{-2} yr^{-1}).
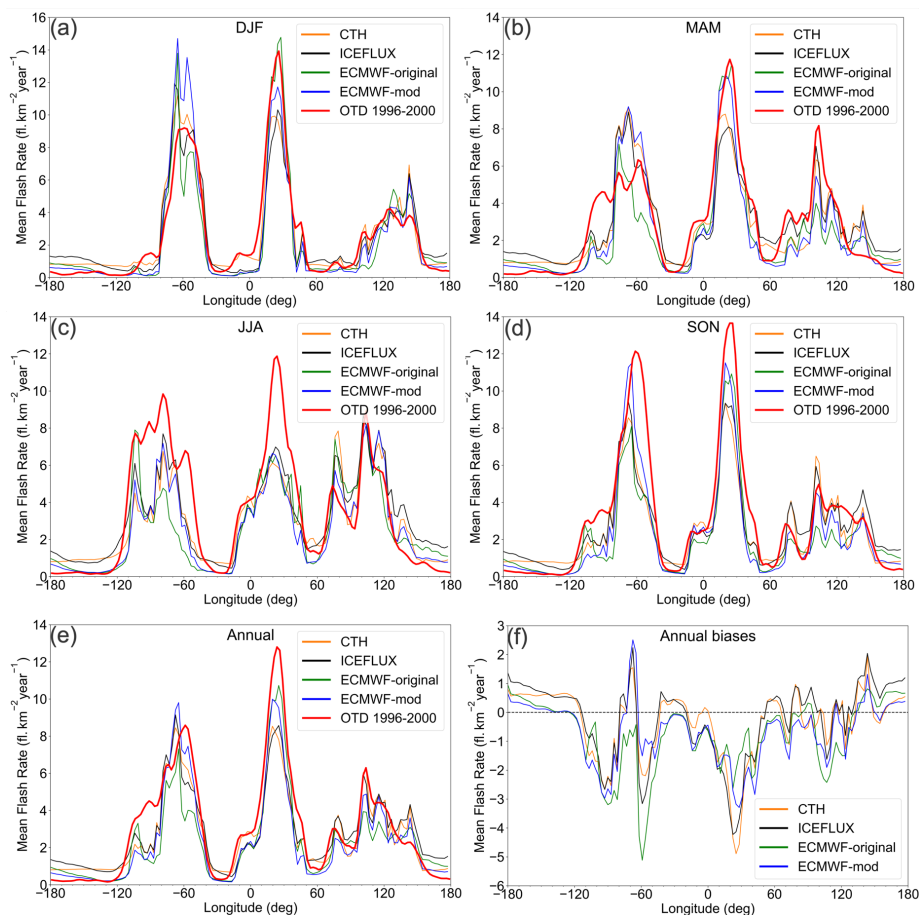
Figure 4: Seasonal and annual meridional average lightning flash densities distribution from OTD 1996–2000 climatology (red line) and from simulation results obtained using different lightning schemes. The meridional average is only taken within the OTD viewing region of ±75° latitude. The biases (model-obs.) in Fig. 4e are also portrayed in Fig. 4f.

Figure 4 displays a comparison of seasonal and annual meridional average lightning flash densities from simulations (2007–2011) and OTD satellite observations (1996–2000). As Fig. 4 shows, the pairs of curves are usually in good agreement, even though the annual plot highlights the underestimation which occurs for Africa (from 0 degrees to 30 degrees east) and North America (from 80 degrees west to 120 degrees west). The ECMWF schemes have made improvements within Africa. Also, the ICEFLUX scheme has slightly reduced the biases over North America. A noticeable underestimation over the Americas in JJA and overestimation in MAM can be observed respectively in Figs. 4c and 4b. Lightning densities over Africa are underestimated to varying degrees in different seasons, with the greatest underestimation occurring in JJA (Fig. 4c). Lightning densities over Asia (from 60 degrees east to 120 degrees east) are slightly underestimated in MAM (Fig. 4b). The ICEFLUX scheme has reduced the biases.
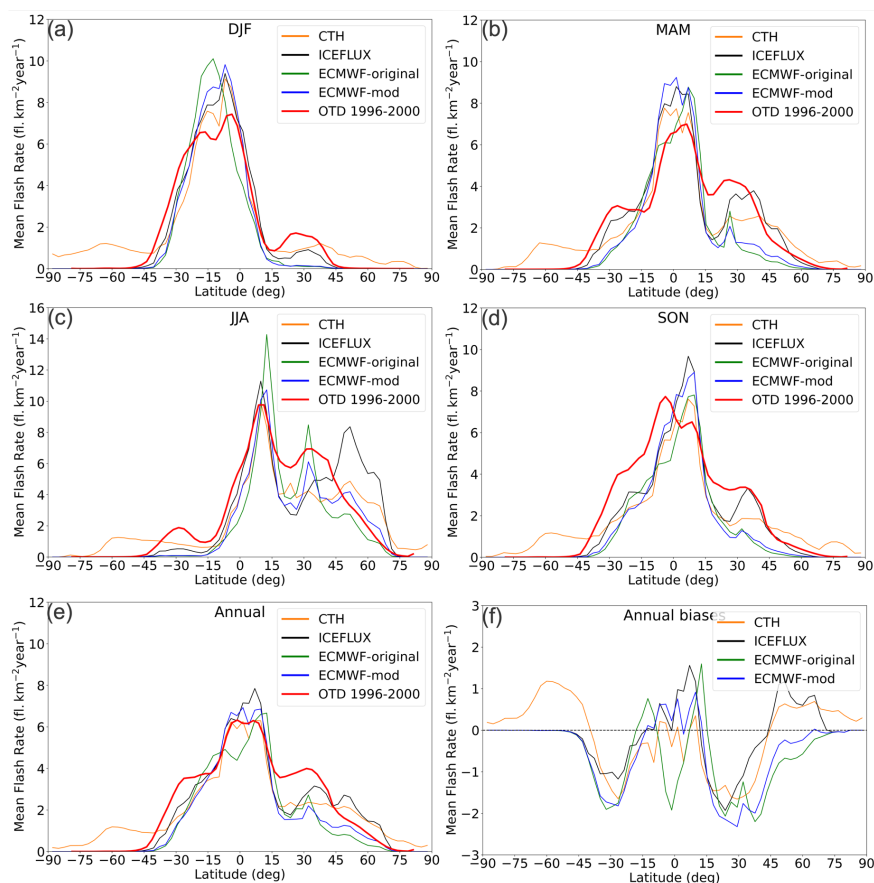
Figure 5: Seasonal and annual zonal average lightning flash densities distribution from OTD 1996–2000 climatology (red line) and from the simulation results obtained using different lightning schemes. The biases (model-obs.) in Fig. 5e are also presented in Fig. 5f.

Figure 5 is the same as Fig. 4, but for the zonal mean distributions. The curves of the model results and the observation results in Fig. 5 show good agreement. Figure 5f shows that, overall, the ICEFLUX scheme and modified ECMWF scheme slightly overestimated the lightning densities near the equator (5°W–5°N). All lightning schemes underestimated the lightning densities within 15°N–45°N and 15°S–45°S. Figure 5f also shows that the ICEFLUX scheme has reduced the biases within 15°N–45°N and 15°S–45°S. Furthermore, Fig. 5f shows that both the ICEFLUX scheme and the CTH scheme overestimated the flash densities within 45°N–90°N. Only the CTH scheme overestimated the flash densities within 45°S–90°S. In DJF (Fig. 5a), all lightning schemes overestimated the flash densities over the low latitude region in the Southern Hemisphere. In MAM (Fig. 5b), lightning densities are overestimated near the equator and underestimated over 15°N–45°N and 15°S–45°S by all lightning schemes to varying degrees. In JJA (Fig. 5c), noticeable overestimation around 10°N by the original ECMWF scheme is apparent. Moreover, the CTH and the original ECMWF schemes respectively facilitated reduction of model biases over 15°S–45°S and 15°N–45°N. Figure 5c also exhibits that the ICEFLUX scheme vastly overestimated the flash densities over 45°N–75°N. As Fig. 5d shows, the model-predicted lightning maximum value is shifted approximately 15 degrees to the north in SON compared to the lightning observations. Figure 5d also shows that all lightning schemes underestimated the lightning densities over 15°N–45°N. The ICEFLUX scheme has shown improvement over this region.

3.2 Validation of LNO$_x$ emissions

3.2.1 Validation of LNO$_x$ emissions by ATom1 and ATom2 observations

To verify the LNO$_x$ emissions of different lightning schemes, we used ATom1 and ATom2 aircraft measurements (NO) for

305 comparison against model results. All lightning schemes, when implemented in CHASER, produce flash rates corresponding to global annual LNO$_x$ emissions within the range estimated by Schumann and Huntrieser (2007) of 2–8 TgN yr^{-1}. To eliminate differences in annual total LNO$_x$ emissions by different lightning schemes, we chose to adjust the annual LNO$_x$ emissions of all lightning schemes to 5.0 TgN yr^{-1} by applying adjustment factors. The "backward C-shaped" LNO$_x$ vertical profile is applied to all lightning schemes.

310
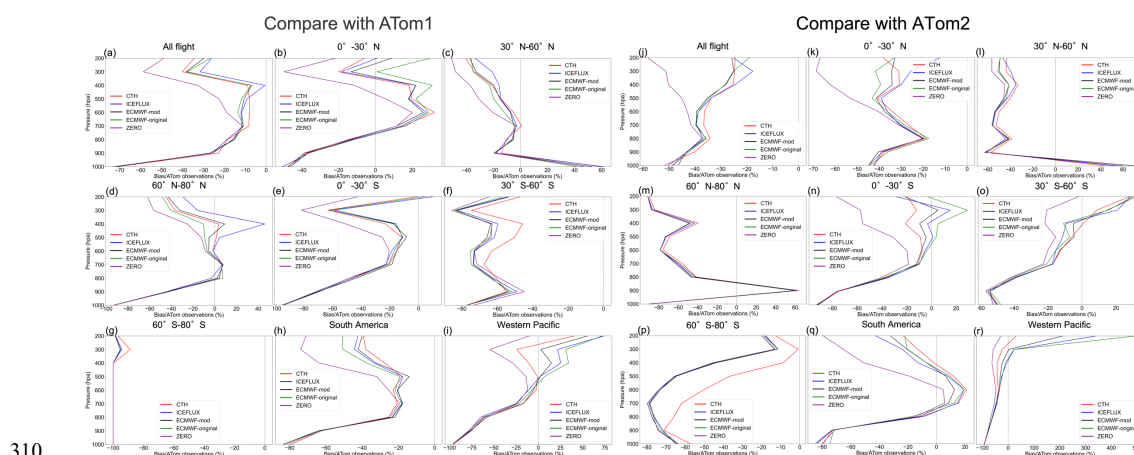
Figure 6: Vertical profile of biases/ATom1 observations (a–i) and the vertical profile of biases/ATom2 observations (j–r). The bias is the model bias against ATom observations. Data for each pressure level P are calculated within the range of $P\pm50$ hPa. South America is the region of 0°–30°S, 0°–30°W. The Western Pacific is the region of 10°N–30°S, 160°E–160°W.

315 **Table 3: Model biases when compared against ATom1 (upper panel) and ATom2 (lower panel). The unit is ppt. The biases within the South America region (0–30°S, 0–30°W) and Western Pacific region (10°N–30°S, 160°E–160°W) are also shown in this table.**

Lightning scheme	All flight	0°–30°N	30°N–60°N	60°N–80°N	0°–30°S	30°S–60°S	60°S–80°S	South America	Western Pacific
CTH	-13.71	-3.56	-15.20	-25.93	-11.24	-15.34	-8.06	-8.09	-5.26
ICEFLUX	-11.43	-2.56	-11.70	-18.98	-10.13	-16.76	-8.29	-8.82	-1.88
ECMWF-mod	-13.06	-0.95	-14.79	-24.86	-10.57	-17.03	-8.31	-8.42	-3.20
ECMWF-original	-12.63	3.90	-15.19	-27.55	-10.62	-17.17	-8.31	-9.89	-1.27
ZERO	-19.00	-11.02	-20.85	-32.98	-15.91	-17.35	-8.34	-13.77	-8.63

Lightning scheme	All flight	0°–30°N	30°N–60°N	60°N–80°N	0°–30°S	30°S–60°S	60°S–80°S	South America	Western Pacific
CTH	-6.95	-8.49	-9.06	-9.46	-9.72	1.25	-3.01	-13.53	-8.29
ICEFLUX	-6.49	-6.38	-9.16	-9.71	-9.87	2.32	-5.39	-24.59	0.94
ECMWF-mod	-7.15	-8.74	-9.95	-9.69	-8.93	2.06	-5.47	-19.02	-2.92
ECMWF-original	-6.59	-9.66	-10.10	-9.82	-2.27	1.89	-5.74	-13.58	3.06
ZERO	-12.66	-15.51	-11.08	-9.77	-28.40	-4.18	-5.94	-47.68	-13.14

Table 3 presents model biases of different lightning schemes against the ATom1 and ATom2 observations. Figure 6 displays the vertical profile of biases/ATom observations in percentage terms. In Table 3 and Fig. 6, case ZERO is the case with the

320 lightning flash, with LNO$_x$ emissions completely switched off. Comparisons between model results and ATom observations were conducted within two specific regions (South America region and Western Pacific region) in which LNO$_x$ is the major source of NO$_x$ (Fig. 7). From comparison of the results simulated using the CTH scheme with the "C-shaped" or the "backward C-shaped" LNO$_x$ vertical profile against ATom measurements, we found that the total model biases were slightly

reduced by application of the "backward C-shaped" LNO_x vertical profile compared to the "C-shaped" LNO_x vertical profile.

325   As Table 3 and Fig. 6 show, the model generally tends to underestimate the NO concentrations. The model biases are reduced considerably by including lightning NO_x sources. For ATom1, overall, the ICEFLUX scheme has the smallest model bias. The ECMWF schemes also reduced the model biases compared to the CTH scheme (Table 3). In the range of 30°S to 80°N in ATom1, the ICEFLUX scheme reduced the model biases considerably. Also, the ECMWF schemes slightly reduced the model biases compared to the CTH scheme (Table 3, Figs. 6a–e). However, in the range of 30°S–80°S, the

330   model biases were slightly extended by the ICEFLUX and the ECMWF schemes compared to the CTH scheme (Table 3, Figs. 6f–g). This finding is consistent with Fig. 5c, in which the lightning densities predicted by the CTH scheme are larger than other lightning schemes in the Southern Hemisphere in JJA. For ATom2, overall, the ICEFLUX scheme and the original ECMWF scheme slightly reduced the model biases over the upper troposphere, compared to the CTH scheme (Fig. 6j). The model biases were reduced by the ICEFLUX scheme over the low latitude region but were extended over the

335   middle-latitude to the high-latitude region compared to the CTH scheme (Figs. 6k–p). The model biases were mostly reduced or extended over the middle to upper troposphere (Fig. 6). This is true because most LNO_x was distributed over the middle to upper troposphere. Also, NO_x has a longer lifetime over the middle to upper troposphere. In the Western Pacific region, results obtained from comparisons with ATom1 and ATom2 indicate that the CTH scheme underestimated, and the other schemes overestimated LNO_x emissions in the upper troposphere; also, both the ICEFLUX scheme and ECMWF

340   schemes reduced the total model biases considerably more than the CTH scheme did.
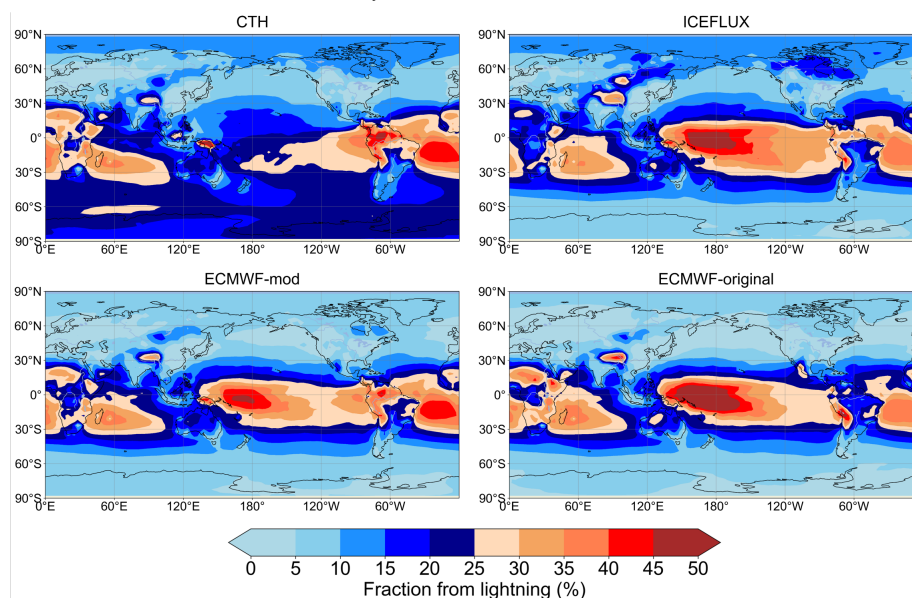
Figure 7: Sensitivity of simulated tropospheric NO_2 columns to LNO_x emissions using different lightning schemes. NO_2 column because of LNO_x emissions was determined as the difference between the simulation with LNO_x emissions and a simulation that excludes LNO_x emissions.

345

3.2.2 Validation of LNO_x emissions by TROPOMI satellite observations

TROPOMI satellite observations of NO_2 tropospheric columns were used to verify LNO_x emission results obtained using the CHASER model. To eliminate differences in annual total LNO_x emissions attributable to the different lightning schemes, we adjusted the annual LNO_x emissions of all lightning schemes to 5.0 TgN yr^{-1} using different adjustment factors. For direct

350   comparison between CHASER and TROPOMI NO_2 tropospheric columns, the averaging kernel information from TROPOMI observations was used. The averaging kernels were applied to CHASER outputs following Eq. (15).

1

$$X_{chaser} = \sum_{i=1}^{N} A_{tropomi} x_{chaser} \tag{15}$$

In that equation, X_{chaser} represents the CHASER NO_2 tropospheric column after averaging kernels applied, $A_{tropomi}$ denotes the TROPOMI averaging kernels, x_{chaser} denotes the CHASER NO_2 partial column at layer i, and N denotes the number of tropospheric layers.
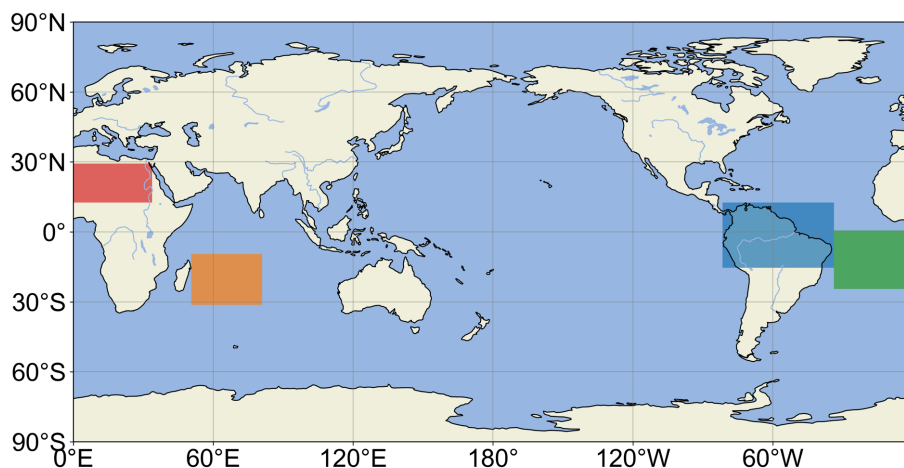
Figure 8: Four target regions for which LNO_x is the major source of NO_x. The four target regions are North Africa (red), Indian Ocean (yellow), Amazon (blue), and South Atlantic (green).
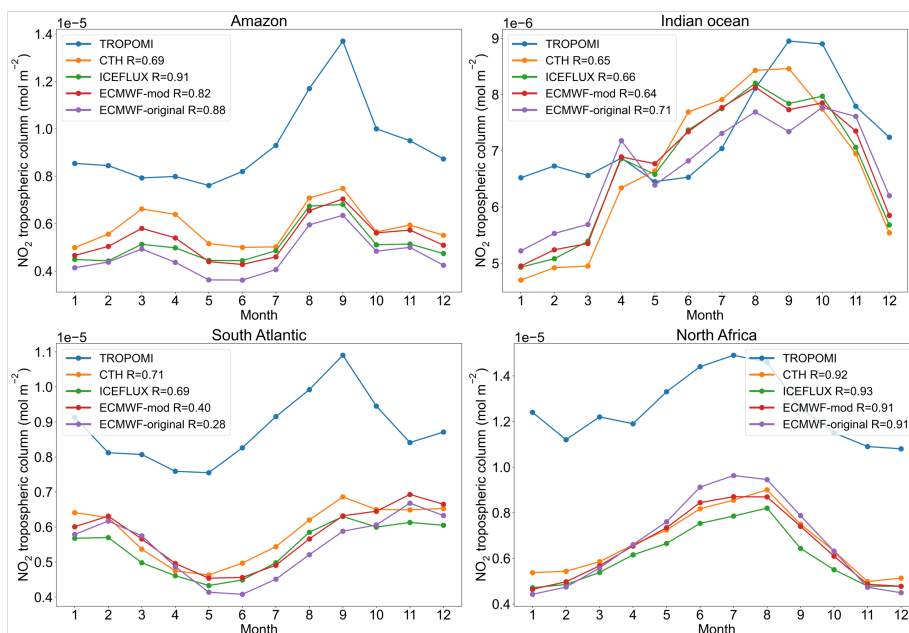
Figure 9: Comparisons of smoothed CHASER and TROPOMI (blue) NO_2 tropospheric columns over four target regions in 2019. Legends show the temporal correlation coefficients.

Comparison between TROPOMI observations and CHASER outputs indicates that the CHASER model tends to underestimate NO_2 tropospheric columns. Overall, the ICEFLUX scheme has shown the smallest model bias of NO_2 tropospheric columns. To validate the results further and to compare the LNO_x emissions of different lightning schemes by TROPOMI observations, four regions are chosen as target regions (Fig. 8), where LNO_x is the major source of NO_x. Figure 7 shows the sensitivity of tropospheric NO_2 columns to LNO_x emissions as simulated using different lightning schemes. As

370 Fig. 7 shows, the four regions presented in Fig. 8 are hotspots for LNOₓ emissions. Therefore, these four regions are chosen as the target regions. Figure 9 presents a comparison of smoothed CHASER and TROPOMI NO_2 tropospheric columns over four target regions in 2019. The spatial average values of each month in 2019 are shown in Fig. 9. That figure shows, generally, the model captured the temporal variation of NO_2 tropospheric columns, especially in the land region (Amazon and North Africa). The ICEFLUX scheme showed good temporal correlation in all four regions, with improved temporal correlation coefficients for three of them (Amazon, Indian Ocean, North Africa) compared to the CTH scheme. The

375 ECMWF schemes have similar temporal correlation coefficients to the CTH scheme in two target regions (Indian Ocean, North Africa). Compared with the CTH scheme, the ECMWF schemes improved the temporal correlation coefficients in the Amazon region considerably. However, the ECMWF schemes reduced the temporal correlation coefficients in the South Atlantic region, mainly because of inconsistency between the model and the observed trends during April–June.

3.3 Effects of different lightning schemes on tropospheric chemical fields

380 In the tropospheric chemical field, LNOₓ has an important role. The LNOₓ effects on the tropospheric chemical fields vary along with differences in the horizontal distribution of LNOₓ in different lightning schemes. To evaluate the influences of different lightning schemes on the tropospheric chemical fields, several ten-year (2011–2020) experiments were conducted with the ten-year mean LNOₓ production of all lightning schemes adjusted to 5.0 TgN yr^{-1} (Section 2.4). CTH scheme with a "backward C-shaped" profile is regarded as the base scheme. The effects of different lightning schemes on the atmospheric

385 chemistry are calculated as shown in Eq. (16).

$$Impact_{ij} = \frac{(LS_{ij} - Base_j)}{Base_j} \qquad (16)$$

Therein, $Impact_{ij}$ represents the effects of the i-th lightning scheme on the concentrations of target atmospheric component j. Also, LS_{ij} denotes the concentrations of target atmospheric component j simulated by the i-th lightning scheme. $Base_j$

390 stands for the concentrations of target atmospheric component j as simulated using the base scheme.
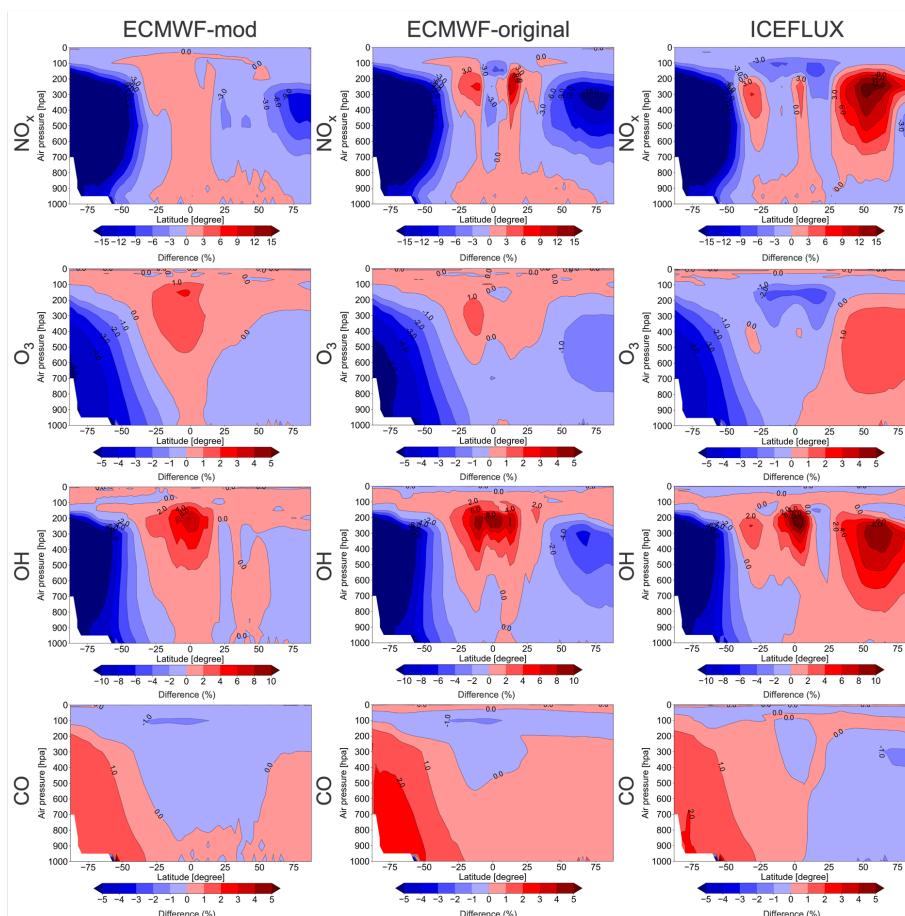
Figure 10: Effects of modified ECMWF scheme, original ECMWF scheme, and ICEFLUX scheme on the atmospheric chemical fields (NOₓ, O₃, OH, CO) on the zonal mean (%).

Figure 10 presents the respective effects of the modified ECMWF, original ECMWF, and ICEFLUX schemes on the atmospheric chemical fields (NO_x, O_3, OH, CO) relative to the base scheme CTH. The modified ECMWF scheme led to an increase (approx. 3%) in NO_x concentration at low latitude regions and a decrease (approx. 15%) at middle to high latitude regions. In the case of the modified ECMWF scheme, the concentration of ozone and OH radical mostly increased at low latitude regions and decreased at middle to high latitude regions in the Southern Hemisphere, which corresponds to the changing pattern of NO_x. Compared to the modified ECMWF scheme, the original ECMWF scheme caused a decrease rather than an increase in ozone and OH radical concentrations in the lower troposphere at low latitude regions. Unlike the modified ECMWF scheme, overall, the original ECMWF scheme led to an increase in CO. As Fig. 10 shows, the three lightning schemes led to a marked decrease in NO_x, O_3, and OH radical concentrations over the South Pole region. This decrease occurred because the lightning densities and the LNO_x emissions simulated by the CTH scheme are markedly higher than those simulated using other lightning schemes at this latitude band (Fig. 2 and Fig. 5e). Moreover, NO_x can engender the formation of ozone and OH radical. In the case of the ICEFLUX scheme, the concentrations of NO_x, ozone, and OH radical mostly increased in the Northern Hemisphere and decreased in the Southern Hemisphere.

Methane lifetime is an indicator reflecting the tropospheric oxidation capacity. The global mean tropospheric lifetime of methane against tropospheric OH radical spanning 2011–2020 with the CTH, original ECMWF, modified ECMWF, and ICEFLUX schemes are estimated respectively as 9.623 years, 9.647 years, 9.612 years, and 9.606 years. Compared to the

CTH scheme, the original ECMWF scheme led to a slight increase in methane's global mean tropospheric lifetime. In contrast, the modified ECMWF and ICEFLUX schemes led to a slight decrease in methane's global mean tropospheric lifetime. Although little difference exists in the total tropospheric oxidation capacity simulated by different lightning

415 schemes, the ECMWF schemes and ICEFLUX scheme led to marked changes of oxidation capacity in different regions of the troposphere.

3.4 Long-term trend analysis of lightning density

The accuracy of predicting the simulated lightning distribution under the current climate is only one aspect of lightning scheme evaluation. The ability of the lightning scheme to reproduce the trend of lightning under climate change is also an

420 important factor. For this study, 20 years of (2001–2020) experiments were conducted to analyze the long-term trends of lightning flash rates simulated using different lightning schemes (section 2.4).
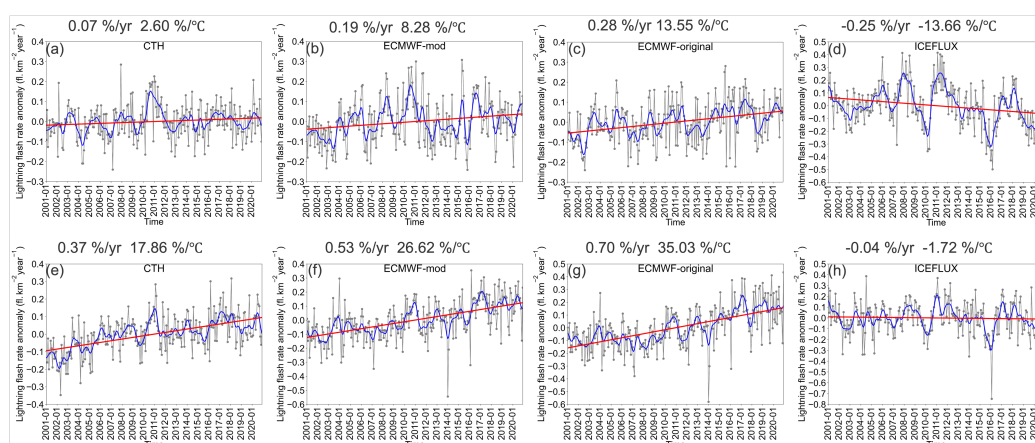
Figure 11: Global anomaly of lightning flash rates calculated from simulation results (2001–2020) using different lightning schemes. Figures 11(a–d) presents results without nudging; Figs. 11(e–h) presents results with nudging.

425

Table 4: Changes in global mean surface temperature (ΔTS), global mean lightning flash rate (ΔLFR), and the rate of change of lightning flash rate corresponding to each degree Celsius increase in global mean surface temperature (ΔLFR/ΔTS). The upper panel shows results obtained without nudging. The lower panel presents results obtained with nudging. Changes were obtained by calculating the difference between the rightmost and leftmost points of the approximating curve for the 2001–2020 time-series data.

Lightning scheme	ΔTS (°C)	ΔLFR (%)	ΔLFR/ΔTS (%/°C)
CTH	0.39	1.03	2.60
ECMWF-mod	0.37	3.08	8.28
ECMWF-original	0.41	5.50	13.55
ICEFLUX	0.38	-5.18	-13.66
Lightning scheme	ΔTS (°C)	ΔLFR (%)	ΔLFR/ΔTS (%/°C)
CTH	0.39	7.04	17.86
ECMWF-mod	0.39	10.49	26.62
ECMWF-original	0.39	13.77	35.03
ICEFLUX	0.39	-0.68	-1.72

430

Figure 11 shows the global anomaly of lightning flash rates calculated from the simulation results. Because nudging to meteorological reanalysis data cannot be used when predicting lightning trends under future climate changes, we also showed the results without nudging. We used the Mann–Kendall rank statistic to ascertain whether the lightning trends in Fig. 11 are significant (Hussain et al., 2019). From results of the Mann–Kendall rank statistic test (significance set as 5%),

all the trends in Fig. 11 were inferred as significant except for the case of the ICEFLUX scheme with nudging applied. As Fig. 11 shows, all lightning schemes predicted increasing trends of lightning except the ICEFLUX scheme, which predicted a decreasing lightning trend. These results are consistent with those of earlier studies (Price and Rind, 1994; Zeng et al., 2008; Jiang and Liao, 2013; Banerjee et al., 2014; Krause et al., 2014; Clark et al., 2017; Finney et al., 2018), which reported that the CTH scheme predicted a 5%–16% increase of lightning flashes per degree of increase in global mean surface temperatures and which reported that the ICEFLUX scheme predicted a 15% decrease of total lightning flash rates in 2100 under Representative Concentration Pathway 8.5 (RCP8.5). The positive lightning trends are generally enhanced by application of meteorological nudging. Few studies have specifically examined the lightning trends predicted by the ECMWF schemes under global warming. When nudging was not applied, the ECMWF schemes predicted the increasing trends of lightning flash rates under global warming by factors of 3 (modified ECMWF scheme) and 5 (original ECMWF scheme) compared to the CTH scheme (Table 4).
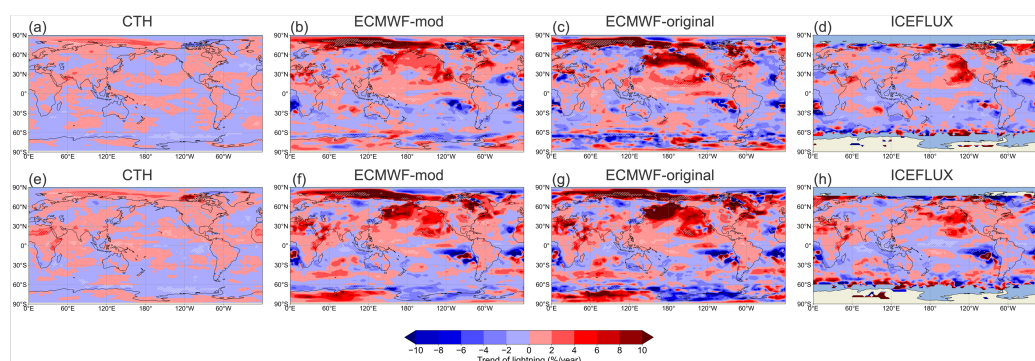
Figure 12: Changes in the lightning flash rate (% yr^{-1}) during 2001–2020 on the two-dimensional map. Changes at every point were calculated from the function of approximating curve for the 2001–2020 time-series data at each grid cell. Figures 12(a–d) show results without nudging; Figs. 12(e–h) show results with nudging.

Figure 12 shows a global map of changes in the lightning flash rate (% yr^{-1}) during 2001–2020. In Fig. 12, the area in which the trend was found to be significant by the Mann–Kendall rank statistic test (significance level inferred for 5%) is marked with hatched lines. As Fig. 12 shows, the distribution of trends simulated by the same lightning scheme is similar whether meteorological nudging was applied or not. As displayed in Fig. 12, in the Arctic region of the Eastern Hemisphere, both the CTH scheme and the ECMWF schemes showed an increasing trend of lightning. Earlier studies based on the World Wide Lightning Location Network (WWLLN) lightning observations have indicated that lightning densities in the Arctic increase concomitantly with increasing global mean surface temperature (Holzworth et al., 2021). Earlier studies indicate that the results of the CTH scheme and the ECMWF schemes are reasonable for the Arctic region of the Eastern Hemisphere. In the high latitude region of the Southern Hemisphere (60°S–70°S), both the CTH scheme and the ECMWF schemes showed decreasing lightning trends. Lightning is rarely observed south of 60°S (Kelley, 2018). Moreover, the trends of lightning in this region expected to occur with global warming remain highly uncertain. In some parts of the Northern Pacific Ocean, the ECMWF schemes and ICEFLUX scheme results showed increasing trends of lightning, which is consistent results obtained from an earlier study (Walter and Buechler, 2008). All schemes show decreasing trends for lightning flash rates in Indonesia, although only the ICEFLUX scheme passed the significance test. In the North Atlantic, all schemes showed increasing lightning trends. Only the CTH scheme failed the significance test.

3.5 Effects of LNO$_x$ emissions on trends of tropospheric O$_3$ and NO$_x$ columns

The long-term trends of lightning densities during 2001–2020 calculated using different lightning schemes have been discussed in section 3.4. Increasing or decreasing trends of lightning can engender corresponding trends of LNO$_x$ emissions, which can consequently influence trends of NO$_x$ and O$_3$ concentrations. To ascertain the extent to which the LNO$_x$ emissions

470   influence NO$_x$ and O$_3$ concentration trends, the effects of the LNO$_x$ emissions on the trends of tropospheric NO$_x$ and O$_3$
columns have been estimated and discussed. We conducted two sets of experiments (section 2.4), one of which interactively
calculated LNO$_x$ emission rates, whereas the other one maintained the 2001 LNO$_x$ emission rates for simulations of the
entire 20 years. The LNO$_x$ emission effects on the trends of tropospheric NO$_x$ and O$_3$ columns can be estimated
quantitatively by comparing the results of these two sets of experiments.
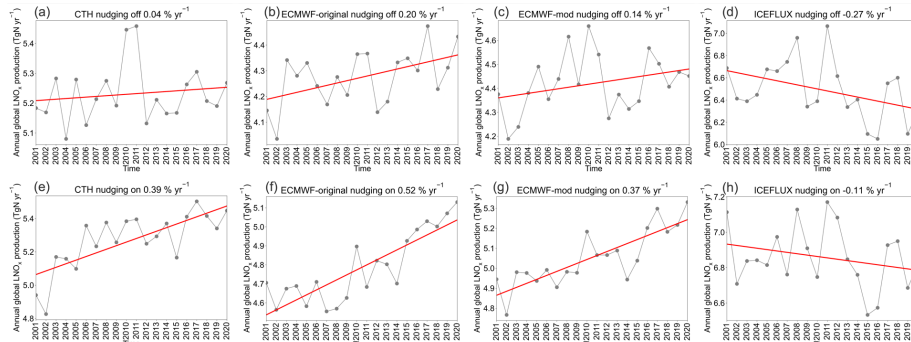
475

Figure 13: Trends of annual global LNO$_x$ emissions calculated from simulation results (2001–2020) from different lightning schemes. Red lines are fitting curves. Figures 13(a–d) present results without nudging; Figs. 13(e–h) present results with nudging. The number in the title of each figure represents the trend corresponding to that figure in the unit of % yr^{-1}.

480   Figure 13 presents trends of annual global LNO$_x$ emissions calculated from the simulation results (2001–2020) obtained
using different lightning schemes. As Fig. 13 shows, the annual global LNO$_x$ emission trends correspond to the trends of
lightning presented in Fig. 11. Similarly to the trends found for lightning, the trends of annual global LNO$_x$ emissions are
also increased by application of meteorological nudging. Only the ICEFLUX scheme simulated decreasing trends of annual
global LNO$_x$ emissions.
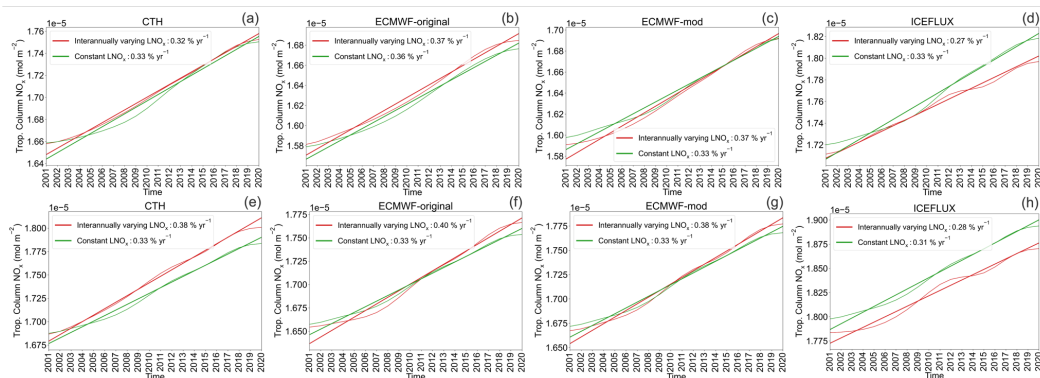
485

Figure 14: Trends of global mean tropospheric NO$_x$ columns calculated from simulation results (2001–2020) using different lightning schemes. Straight lines in the figure are the fitting curves. Straight lines and curves in red are results calculated using the first set of experiments. Straight lines and curves in green show results calculated using the second set of experiments (Table 2). The numbers in legends represent trends corresponding to that figure in the unit of % yr^{-1}. Figures 14(a–d) present results obtained without
490   **nudging; Figs. 14(e–h) present results obtained without nudging.**

Figure 14 portrays trends of global mean tropospheric NO$_x$ columns calculated from the first and second set of experiments
(Table 2). As Fig. 13 and Fig. 14 depict, when the trends of annual global LNO$_x$ emissions are not strong (e.g., Fig. 13a),
their effects on the trends of global mean tropospheric NO$_x$ columns are negligible. The marked increasing trends of annual
495   global LNO$_x$ emissions (Figs. 13e, f, g) led to great increases (15.2%–21.2%) of the increasing trends of tropospheric NO$_x$
columns (Figs. 14e, f, g). In the case of ICEFLUX, because of the decreasing trends of LNO$_x$ emissions, the increasing
trends of the tropospheric NO$_x$ columns decreased by around 10%.
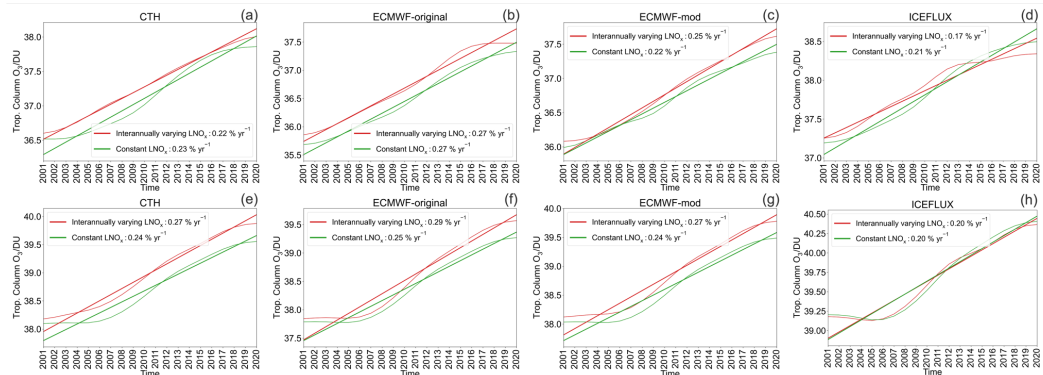
Figure 15: Trends of global mean tropospheric O₃ columns calculated from simulation results (2001–2020) using different lightning schemes. Straight lines in the figure are the fitting curves. Straight lines and curves in red are results calculated using the first set of experiments. Straight lines and curves in green are results calculated using the second set of experiments (Table 2). The number in the legend represents the trend corresponding to that figure in the unit of % yr⁻¹. Figures 15(a–d) present results obtained without nudging; Figs. 15(e–h) show results obtained with nudging.

Figure 15 is similar to the results shown in Fig. 14, but for tropospheric O_3 columns. Because NO_x causes the formation of O_3 by the fundamental chemical cycle of O_x–NO_x–HO_x, the trends of the global mean tropospheric O_3 columns are affected strongly by trends of the global mean tropospheric NO_x columns. For CTH and the original ECMWF schemes without nudging (Figs. 14a, b and Figs. 15a, b), the simulated trends of tropospheric O_3 columns are almost identical because the trends of tropospheric NO_x columns simulated by the two sets of experiments are very similar. As Fig. 13 and Fig. 15 show, the marked increasing trends of annual global LNO_x emissions led to increases of the increasing trends of tropospheric O_3 columns by around 15% (Figs. 15e, f, g). In the case of ICEFLUX without nudging, because of the decreasing trend of LNO_x emissions, the increasing trend of the tropospheric O_3 columns decreased by around 20% (Fig. 15d).
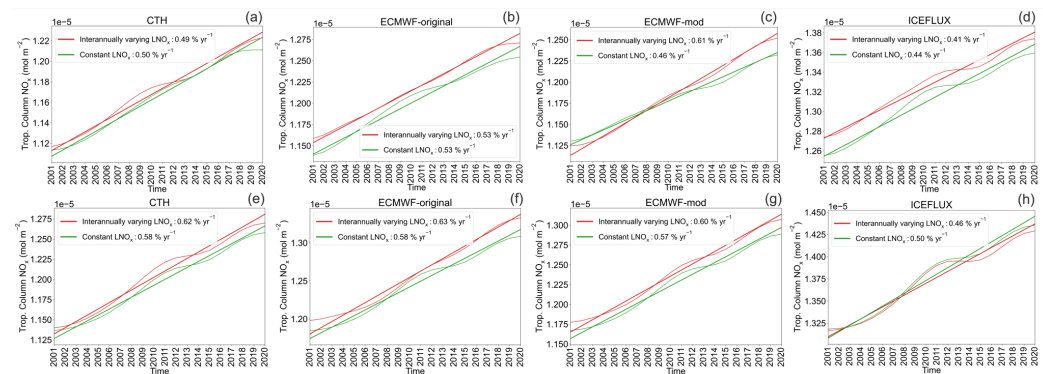
Figure 16: Trends of North Pacific region (10°S–60°N; 150°E–240°E) mean tropospheric NOₓ columns calculated from simulation results (2001–2020) by different lightning schemes. Straight lines in the figure are the fitting curves. Straight lines and curves in red are results calculated using the first set of experiments. Straight lines and curves in green are results calculated using the second set of experiments (Table 2). The number in the legend represents the trend corresponding to that figure in the unit of % yr⁻¹. Figures 16(a–d) present results obtained without nudging; Figs. 16(e–h) present results obtained with nudging.
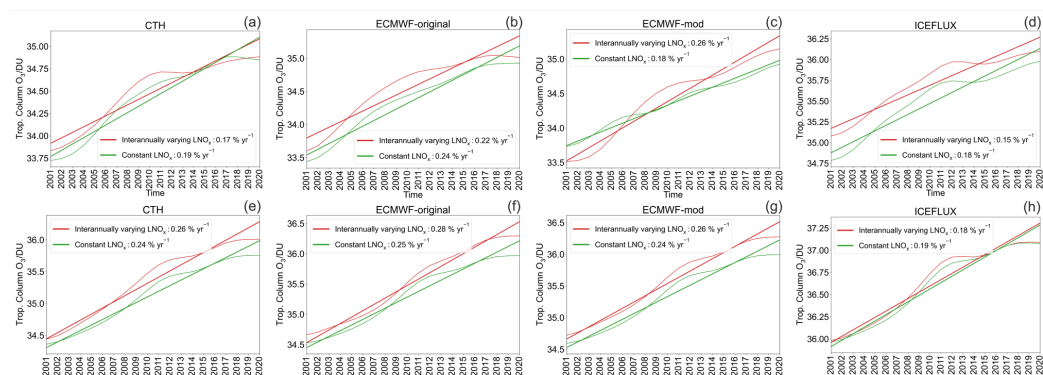
520 **Figure 17: Trends of North Pacific region (10°S–60°N; 150°E–240°E) mean tropospheric O₃ columns calculated from the simulation results (2001–2020) by different lightning schemes. Straight lines in the figure are the fitting curves. Straight lines and curves in red are the results calculated using the first set of experiments. Straight lines and curves in green are the results calculated using the second set of experiments (Table 2). The number in the legend represents the trend corresponding to that figure in the unit of % yr⁻¹. Figures 17(a–d) show the results obtained without nudging; Figs. 17(e–h) show the results obtained with nudging.**

525

As discussed in Section 3.4, lightning densities increased or decreased to a considerable degree in different regions of the world, as simulated by all the introduced lightning schemes (Fig. 12). We chose to investigate the LNO_x emission effects on the tropospheric NO_x and O_3 column trends over a region with greatly increasing LNO_x, as simulated by the ECMWF schemes (North Pacific region 10°S–60°N; 150°E–240°E). Figure 16 shows trends of North Pacific region (10°S–60°N;

530 150°E–240°E) mean tropospheric NO_x columns calculated from the first and second set of experiments (Table 2). Figure 17 is similar to the graphic presented in Fig. 16, but for tropospheric O_3 columns. In the case of the modified ECMWF scheme without nudging (Fig. 16c and Fig. 17c), because of the increasing trend of LNO_x emissions, the trends of tropospheric NO_x and O_3 columns increased significantly by 32.6% and 44.4%, respectively. However, although the LNO_x emissions increased significantly in the case of the original ECMWF scheme without nudging, the trends simulated by the first and second set of

535 experiments are almost identical (Fig. 16b). This close approximation might be attributable to the different meteorological conditions and chemical fields during simulations.

In conclusion, because the ICEFLUX scheme predicts the opposite trends of LNO_x emissions from the other lightning schemes, they simulate opposite effects on the long-term trends of global mean tropospheric NO_x and O_3 columns.

540 Furthermore, an evident trend of annual global (regional) LNO_x emissions has a strong effect on the trend of global (regional) mean tropospheric NO_x and O_3 columns.

4 Conclusions

Two new lightning schemes, the ICEFLUX and the original ECMWF schemes, were implemented into CHASER (MIROC), a global chemical climate model. By modifying the equations and adjustment factors from the original ECMWF scheme

545 based on work reported by McCaul et al. (2009), a new modified ECMWF scheme was also tested with CHASER (MIROC).

Using OTD lightning observations as validation data, both the ICEFLUX and ECMWF schemes simulated the spatial distribution of lightning more accurately on a global scale than the CTH scheme did, the lightning distribution in the ocean region was especially improved. The modified ECMWF scheme showed the highest prediction accuracy for the spatial

550 distribution of lightning on a global scale.

To verify the LNO_x emissions of different lightning schemes, we used NO observations from ATom1 and ATom2. Overall, both the ICEFLUX scheme and the ECMWF schemes reduced the model biases compared to the CTH scheme, except in the case of comparison between the modified ECMWF scheme and ATom2 observations. Although both the ICEFLUX scheme

555 and the ECMWF schemes reduced the model biases, the ICEFLUX scheme reduced the biases to a greater degree. Comparison of the model results with ATom1 observations revealed that the ICEFLUX scheme has the lowest model biases at 30°S–80°N, whereas the CTH scheme has the lowest model biases at 30°S–80°S. When comparing the model outputs with ATom2 observations, the ICEFLUX scheme has the smallest model biases at low latitude region (30°S–30°N). Results show that the CTH scheme has the smallest model biases at middle-latitude to high-latitude regions.

560

We also used TROPOMI NO_2 tropospheric columns to verify the LNO_x emissions of different lightning schemes. Compared with the CTH scheme, the ICEFLUX scheme reduced the global mean model bias, whereas the ECMWF schemes increased the global mean model bias, which indicates that the ICEFLUX scheme improved the LNO_x simulation accuracy in the model. In the four target regions where LNO_x is the dominant source of NO_x, the ICEFLUX scheme is the best lightning

565 scheme able to capture the seasonal variation of NO_2, whereas the ECMWF schemes only significantly improved the temporal correlations between the model and the TROPOMI observations in the Amazon region.

Effects of the newly implemented lightning schemes on the tropospheric chemical fields are evaluated compared to the CTH scheme. Compared with the CTH scheme, the ECMWF schemes mainly led to a slight increase in NO_x, ozone, and OH

570 radical concentrations at low latitude regions and a decrease at middle-latitude to high-latitude regions. Effects of the ICEFLUX scheme on the tropospheric chemical fields differ from those of the ECMWF schemes. The ICEFLUX model mainly causes a slight increase of NO_x, ozone, and OH radical concentrations in the Northern Hemisphere and a decrease in the concentrations of the three chemical species in the Southern Hemisphere. Commonality between the ECMWF schemes and the ICEFLUX scheme is that they both result in decreasing concentrations of NO_x, ozone, and OH radical at the middle

575 to high latitude regions of the Southern Hemisphere. Although the newly implemented lightning schemes have little effect on the total oxidation capacity of the troposphere compared to the CTH scheme, they led to marked change of oxidation capacity in different regions of the atmosphere.

This study also analyzed the long-term trends of lightning simulated by different lightning schemes under global warming

580 during 2001–2020. All the lightning schemes predicted increasing lightning trends except the ICEFLUX scheme, which predicted a decreasing lightning trend. The Mann–Kendall rank statistic was used to ascertain whether the lightning trends were significant. Use of Mann–Kendall rank statistic tests revealed that all the lightning trends are significant, except the ICEFLUX scheme with nudging applied, for significance at 5%. Moreover, findings showed that when nudging was not applied, the ECMWF schemes predicted an increasing trend of lightning flash rate under global warming by factors of 3

585 (modified ECMWF scheme) and 5 (original ECMWF scheme) compared to the CTH scheme.

Finally, we quantitatively estimated the LNO_x emission effects on tropospheric NO_x and O_3 column trends during 2001–2020. Results showed that a marked trend of annual global (regional) LNO_x emissions significantly affects the trend of global (regional) mean tropospheric NO_x and O_3 columns.

590

In summary, comparison with results obtained using the CTH scheme demonstrated that both the ICEFLUX and ECMWF schemes improved the prediction accuracy of the lightning distribution on a global scale. In fact, the modified ECMWF scheme has the highest prediction accuracy. Using ATom aircraft observations and TROPOMI satellite observations to verify the LNO_x emissions, the results show that, compared to the CTH scheme, the ICEFLUX scheme reduced the model

595   biases to a greater degree than the ECMWF schemes. Although a considerable degree of uncertainty remains in the

prediction of lightning trends under global warming, results of most studies have indicated that the global average lightning

density can be expected to increase by about 10% for each degree of global warming (Betz et al., 2008, p. 521). This value is

most consistent with the lightning increase rate predicted by the modified ECMWF scheme without nudging in this study.

Future research should be undertaken for specific examination of development of lightning schemes that both accurately

600   predict the global distribution of LNO_x and which predict the changes in lightning that are expected to occur concomitantly

with global climate change.

Code availability

The source code for CHASER to reproduce results in this work is obtainable from the repository at
https://doi.org/10.5281/zenodo.5835796 (He et al., 2022)

605   **Data availability**

The LIS/OTD data used for this study are available from https://ghrc.nsstc.nasa.gov/hydro/?q=LRTS (last access: 11 January
2022). The ATom data used for this study are available from https://daac.ornl.gov/ATOM/guides/ATom_merge.html (last
access: 11 January 2022). The TROPOMI data used for this study are available from
https://s5phub.copernicus.eu/dhus/#/home (last access: 11 January 2022).

610   **Author contribution**

YFH introduced new lightning schemes into CHASER (MIROC) by adding new codes to CHASER (MIROC), conducted all
simulations, interpreted the results, and wrote the manuscript. KS developed the model code, conceived of the presented
idea, and supervised the findings of this work and the manuscript preparation. HMSH provided the TROPOMI data and the
relevant codes to pre-process the TROPOMI data.

615   **Competing interests**

The authors declare that they have no conflict of interest.

Acknowledgements

This research was supported by the Global Environment Research Fund (S–12 and S–20) of the Ministry of the Environment
(MOE), Japan, and JSPS KAKENHI Grant Numbers: JP20H04320, JP19H05669, and JP19H04235. This work was
620   supported by Japan Science and Technology Agency (JST) Support for Pioneering Research Initiated by the Next Generation
(SPRAING), Grant Number JPMJSP2125. The author (Initial) would like to take this opportunity to thank the
"Interdisciplinary Frontier Next-Generation Researcher Program of the Tokai Higher Education and Research System." The
simulations were completed with the supercomputer (NEC SX-Aurora TSUBASA) at NIES (Japan). Thanks to NASA
scientists and staff for providing LIS/OTD lightning observation data
625   (https://ghrc.nsstc.nasa.gov/uso/ds_docs/lis_climatology/LISOTD_climatology_dataset.html, last access: 9 January 2022)
and ATom data (https://espo.nasa.gov/atom/content/ATom, last access: 9 January 2022). We are grateful to ESA scientists
and staff for providing TROPOMI data (http://www.tropomi.eu, last access: 9 January 2022). We thank Yannick Copin for
software he developed to help us with the Taylor diagram.

References

630   Banerjee, A., Archibald, A. T., Maycock, A. C., Telford, P., Abraham, N. L., Yang, X., Braesicke, P., and Pyle, J. A.:

Lightning NO_x, a key chemistry-climate interaction: impacts of future climate change and consequences for tropospheric

oxidising capacity, Atmos. Chem. Phys, 14, 9871–9881, https://doi.org/10.5194/acp-14-9871-2014, 2014.

Betz, H. D., Schumann, U., and Laroche, P.: Lightning: Principles, instruments and applications: Review of modern

635 lightning research, Springer Netherlands, 1–641 pp., https://doi.org/10.1007/978-1-4020-9079-0, 2009.

Cecil, D. J., Buechler, D. E., and Blakeslee, R. J.: Gridded lightning climatology from TRMM-LIS and OTD: Dataset
description, Atmos. Res., 135–136, 404–414, https://doi.org/10.1016/j.atmosres.2012.06.028, 2014.

640 Clark, S. K., Ward, D. S., and Mahowald, N. M.: Parameterization-based uncertainty in future lightning flash density,
Geophys. Res. Lett., 44, 2893–2901, https://doi.org/10.1002/2017GL073017, 2017.

Finney, D. L., Doherty, R. M., Wild, O., Huntrieser, H., Pumphrey, H. C., and Blyth, A. M.: Using cloud ice flux to
parametrise large-scale lightning, Atmos. Chem. Phys., 14, 12665–12682, https://doi.org/10.5194/acp-14-12665-2014, 2014.

645

Finney, D. L., Doherty, R. M., Wild, O., Young, P. J., and Butler, A.: Response of lightning NO_x emissions and ozone
production to climate change: Insights from the Atmospheric Chemistry and Climate Model Intercomparison Project,
Geophys. Res. Lett., 43, 5492–5500, https://doi.org/10.1002/2016GL068825, 2016a.

650 Finney, D. L., Doherty, R. M., Wild, O., and Abraham, N. L.: The impact of lightning on tropospheric ozone chemistry using
a new global lightning parametrisation, Atmos. Chem. Phys., 16, 7507–7522, https://doi.org/10.5194/acp-16-7507-2016,
2016b.

Finney, D. L., Doherty, R. M., Wild, O., Stevenson, D. S., MacKenzie, I. A., and Blyth, A. M.: A projected decrease in

655 lightning under climate change, Nat. Clim. Chang., 8, 210–213, https://doi.org/10.1038/s41558-018-0072-6, 2018.

Grewe, V.: Impact of climate variability on tropospheric ozone, Sci. Total Environ., 374, 167–181,
https://doi.org/10.1016/j.scitotenv.2007.01.032, 2007.

660 Ha, P. T. M., Matsuda, R., Kanaya, Y., Taketani, F., and Sudo, K.: Effects of heterogeneous reactions on tropospheric
chemistry: A global simulation with the chemistry-climate model CHASER V4.0, Geosci. Model Dev., 14, 3813–3841,
https://doi.org/10.5194/gmd-14-3813-2021, 2021.

He, Y., Hoque, M. S. H., and Sudo, K.: Introducing new lightning schemes into the CHASER (MIROC) chemistry climate

665 model [Code], Zenodo, https://doi.org/10.5281/ZENODO.5835796, 2022.

Holzworth, R. H., Brundell, J. B., McCarthy, M. P., Jacobson, A. R., Rodger, C. J., and Anderson, T. S.: Lightning in the
Arctic, Geophys. Res. Lett., 48, e2020GL091366, https://doi.org/10.1029/2020GL091366, 2021.

670 Hui, J. and Hong, L.: Projected Changes in NO_x Emissions from Lightning as a Result of 2000–2050 Climate Change,
Atmos. Ocean. Sci. Lett., 6, 284–289, https://doi.org/10.3878/j.issn.1674-2834.13.0042, 2013.

Hussain, M. and Mahmud, I.: pyMannKendall: a python package for non parametric Mann Kendall family of trend tests., J.
Open Source Softw., 4, 1556, https://doi.org/10.21105/joss.01556, 2019.

675

Inness, A., Baier, F., Benedetti, A., Bouarar, I., Chabrillat, S., Clark, H., Clerbaux, C., Coheur, P., Engelen, R. J., Errera, Q.,
Flemming, J., George, M., Granier, C., Hadji-Lazaro, J., Huijnen, V., Hurtmans, D., Jones, L., Kaiser, J. W., Kapsomenakis,
J., Lefever, K., Leitão, J., Razinger, M., Richter, A., Schultz, M. G., Simmons, A. J., Suttie, M., Stein, O., Thépaut, J.-N.,
Thouret, V., Vrekoussis, M., Zerefos, C., and the MACC team: The MACC reanalysis: an 8 yr data set of atmospheric
680   composition, Atmos. Chem. Phys., 13, 4073–4109, https://doi.org/10.5194/acp-13-4073-2013, 2013.

Isaksen, I. S. A. and Hov, Ø.: Calculation of trends in the tropospheric concentration of O_3, OH, CO, CH_4 and NO_x, Tellus B,
39 B, 271–285, https://doi.org/10.1111/j.1600-0889.1987.tb00099.x, 1987.

685   Kelley, O. A., Thomas, J. N., Solorzano, N. N., and Holzworth, R. H.: Fire and Ice: Intense covective precipitation observed
at high latitudes by the GPM satellite's Dual-frequency Precipitation Radar (DPR) and the ground-based World Wide
Lightning Location Network (WWLLN), AGU Poster, 2018, H43F-2487, 2018.

Krause, A., Kloster, S., Wilkenskjeld, S., and Paeth, H.: The sensitivity of global wildfires to simulated past, present, and
690   future lightning frequency, J. Geophys. Res. Biogeosciences, 119, 312–322, https://doi.org/10.1002/2013JG002502, 2014.

Labrador, L. J., von Kuhlmann, R., and Lawrence, M. G.: The effects of lightning-produced NO_x and its vertical distribution
on atmospheric chemistry: sensitivity simulations with MATCH-MPIC, Atmos. Chem. Phys., 5, 1815–1834,
https://doi.org/10.5194/acp-5-1815-2005, 2005.
695
Lamarque, J. F., Shindell, D. T., Josse, B., Young, P. J., Cionni, I., Eyring, V., Bergmann, D., Cameron-Smith, P., Collins,
W. J., Doherty, R., Dalsoren, S., Faluvegi, G., Folberth, G., Ghan, S. J., Horowitz, L. W., Lee, Y. H., MacKenzie, I. A.,
Nagashima, T., Naik, V., Plummer, D., Righi, M., Rumbold, S. T., Schulz, M., Skeie, R. B., Stevenson, D. S., Strode, S.,
Sudo, K., Szopa, S., Voulgarakis, A., and Zeng, G.: The atmospheric chemistry and climate model intercomparison Project
700   (ACCMIP): Overview and description of models, simulations and climate diagnostics, Geosci. Model Dev., 6, 179–206,
https://doi.org/10.5194/gmd-6-179-2013, 2013.

Liaskos, C. E., Allen, D. J., and Pickering, K. E.: Sensitivity of tropical tropospheric composition to lightning NO_x
production as determined by replay simulations with GEOS-5, J. Geophys. Res., 120, 8512–8534,
705   https://doi.org/10.1002/2014JD022987, 2015.

Lopez, P.: A lightning parameterization for the ECMWF integrated forecasting system, Mon. Weather Rev., 144, 3057–
3075, https://doi.org/10.1175/MWR-D-16-0026.1, 2016.

710   McCaul, E. W., Goodman, S. J., LaCasse, K. M., and Cecil, D. J.: Forecasting lightning threat using cloud-resolving model
simulations, Weather Forecast., 24, 709–729, https://doi.org/10.1175/2008WAF2222152.1, 2009.

Murray, L. T.: Lightning NO_x and Impacts on Air Quality, https://doi.org/10.1007/s40726-016-0031-7, 25 April 2016.

715   Ott, L. E., Pickering, K. E., Stenchikov, G. L., Allen, D. J., DeCaria, A. J., Ridley, B., Lin, R. F., Lang, S., and Tao, W. K.:
Production of lightning NO_x and its vertical distribution calculated from three-dimensional cloud-scale chemical transport
model simulations, J. Geophys. Res. Atmos., 115, D04301, https://doi.org/10.1029/2009JD011880, 2010.

Pickering, K. E., Wang, Y., Tao, W. K., Price, C., and Müller, J. F.: Vertical distributions of lightning NOₓ for use in
720   regional and global chemical transport models, J. Geophys. Res. Atmos., 103, 31203–31216,
https://doi.org/10.1029/98JD02651, 1998.

Price, C. and Rind, D.: A simple lightning parameterization for calculating global lightning distributions, J. Geophys. Res.,
97, 9919–9933, https://doi.org/10.1029/92JD00719, 1992.

725

Price, C. and Rind, D.: What determines the cloud-to-ground lightning fraction in thunderstorms?, Geophys. Res. Lett., 20,
463–466, https://doi.org/10.1029/93GL00226, 1993.

Price, C. and Rind, D.: Possible implications of global climate change on global lightning distributions and frequencies, J.
730   Geophys. Res., 99, 823–833, https://doi.org/10.1029/94jd00019, 1994.

Price, C., Penner, J., and Prather, M.: NOₓ from lightning 1. Global distribution based on lightning physics, J. Geophys. Res.
Atmos., 102, 5929–5941, https://doi.org/10.1029/96jd03504, 1997.

735   Romps, D. M.: Evaluating the Future of Lightning in Cloud-Resolving Models, Geophys. Res. Lett., 46, 14863–14871,
https://doi.org/10.1029/2019GL085748, 2019.

Romps, D. M., Seeley, J. T., Vollaro, D., and Molinari, J.: Projected increase in lightning strikes in the united states due to
global warming, Science (80-.)., 346, 851–854, https://doi.org/10.1126/science.1259100, 2014.

740

Schumann, U. and Huntrieser, H.: The global lightning-induced nitrogen oxides source, Atmos. Chem. Phys., 7, 3823–3907,
https://doi.org/10.5194/acp-7-3823-2007, 2007.

Sudo, K. and Akimoto, H.: Global source attribution of tropospheric ozone: Long-range transport from various source
745   regions, 112, https://doi.org/10.1029/2006JD007992, 2007.

Sudo, K., Takahashi, M., Kurokawa, J. I., and Akimoto, H.: CHASER: A global chemical model of the troposphere 1. Model
description, J. Geophys. Res. Atmos., 107, ACH 7-1-ACH 7-20, https://doi.org/10.1029/2001JD001113, 2002.

750   Takemura, T., Egashira, M., Matsuzawa, K., Ichijo, H., O'Ishi, R., and Abe-Ouchi, A.: A simulation of the global
distribution and radiative forcing of soil dust aerosols at the Last Glacial Maximum, Atmos. Chem. Phys., 9, 3061–3073,
https://doi.org/10.5194/acp-9-3061-2009, 2009.

Tost, H.: Chemistry–climate interactions of aerosol nitrate from lightning, Atmos. Chem. Phys., 17, 1125–1142,
755   https://doi.org/10.5194/acp-17-1125-2017, 2017.

Tost, H., Jöckel, P., and Lelieveld, J.: Lightning and convection parameterisations – Uncertainties in global modelling,
Atmos. Chem. Phys., 7, 4553–4568, https://doi.org/10.5194/acp-7-4553-2007, 2007.

760   Walter A. Petersen and D. Buechler: Global tropical lightning trends: Has tropical lightning frequency responded to global
climate change?, in: Third Conference on Meteorological Applications of Lightning Data, New Orleans, USA, 20-28
January 2008, 2.1, 2008

Watanabe, S., Hajima, T., Sudo, K., Nagashima, T., Takemura, T., Okajima, H., Nozawa, T., Kawase, H., Abe, M.,
765   Yokohata, T., Ise, T., Sato, H., Kato, E., Takata, K., Emori, S., and Kawamiya, M.: MIROC-ESM 2010: Model description
and basic results of CMIP5-20c3m experiments, Geosci. Model Dev., 4, 845–872, https://doi.org/10.5194/gmd-4-845-2011,
2011.

Wild, O.: Modelling the global tropospheric ozone budget: Exploring the variability in current models, Atmos. Chem. Phys.,
770   7, 2643–2660, https://doi.org/10.5194/acp-7-2643-2007, 2007.

Wofsy, S. C., Afshar, S., Allen, H. M., Apel, E., Asher, E. C., Barletta, B., Bent, J., Bian, H., Biggs, B. C., Blake, D. R.,
Blake, N., Bourgeois, I., Brock, C. A., Brune, W. H., Budney, J. W., Bui, T. P., Butler, A., Campuzano-Jost, P., Chang, C.
S., Chin, M., Commane, R., Correa, G., Crounse, J. D., Cullis, P. D., Daube, B. C., Day, D. A., Dean-Day, J. M., Dibb, J. E.,
775   Digangi, J. P., Diskin, G. S., Dollner, M., Elkins, J. W., Erdesz, F., Fiore, A. M., Flynn, C. M., Froyd, K., Gesler, D. W.,
Hall, S. R., Hanisco, T. F., Hannun, R. A., Hills, A. J., Hintsa, E. J., Hoffman, A., Hornbrook, R. S., Huey, L. G., Hughes, S.,
Jimenez, J. L., Johnson, B. J., Katich, J. M., Keeling, R., Kim, M. J., Kupc, A., Lait, L. R., Lamarque, J. F., Liu, J., McKain,
K., McLaughlin, R. J., Meinardi, S., Miller, D. O., Montzka, S. A., Moore, F. L., Morgan, E. J., Murphy, D. M., Murray, L.
T., Nault, B. A., Neuman, J. A., Newman, P. A., Nicely, J. M., Pan, X., Paplawsky, W., Peischl, J., Prather, M. J., Price, D.
780   J., Ray, E., Reeves, J. M., Richardson, M., Rollins, A. W., Rosenlof, K. H., Ryerson, T. B., Scheuer, E., Schill, G. P.,
Schroder, J. C., Schwarz, J. P., St. Clair, J. M., Steenrod, S. D., Stephens, B. B., Strode, S. A., Sweeney, C., Tanner, D.,
Teng, A. P., Thames, A. B., Thompson, C. R., Ullmann, K., Veres, P. R., Vizenor, N., Wagner, N. L., Watt, A., Weber, R.,
Weinzierl, B. Wennberg, P, Williamson, C J, Wilson, J C, Wolfe, G M, Woods, C T, Zeng, L H: ATom: Merged
Atmospheric Chemistry, Trace Gases, and Aerosols, https://doi.org/10.3334/ornldaac/1581, 2018.
785

Zeng, G., Pyle, J. A., and Young, P. J.: Impact of climate change on tropospheric ozone and its global budgets, Atmos.
Chem. Phys., 8, 369–387, https://doi.org/10.5194/acp-8-369-2008, 2008.